Pergamon

PII: S0301-9322(96)00007-9

Int. J. Multiphase Flow Vol. 22, No. 4, pp. 667–683, 1996

0301-9322/96 $15.00 + 0.00

LARGE EDDY SIMULATION OF PARTICLE DEPOSITION IN A VERTICAL TURBULENT CHANNEL FLOW

Q. WANG and K. D. SQUIRES

Department of Mechanical Engineering, 209 Votey Building, University of Vermont, Burlington, VT 05405, U.S.A.

(Received 2 January 1995; in revised form 2 February 1996)

Abstract—The deposition of particles in fully-developed turbulent channel flow has been calculated using large eddy simulation of the incompressible Navier–Stokes equations. Calculations were performed for Reynolds numbers of 11,160 and 79,400 (based on bulk velocity and hydraulic diameter); subgrid-scale stresses were parameterized using the dynamic eddy viscosity model. Particle motion was governed by both drag and lift. The effect of particle–particle interactions as well as modification of the turbulent carrier flow by the particles was neglected. In agreement with previous studies, LES results show that particles accumulate in the near-wall region. Statistical measures from the LES calculations such as the particle deposition rate are in reasonable agreement with the direct numerical simulation results of McLaughlin (1989). For particles with identical relaxation times in wall units, deposition rates at the two Reynolds numbers were nearly identical. Issues relevant to application of LES for predicting particle deposition at high Reynolds numbers are also discussed. Copyright © 1996 Elsevier Science Ltd.

Key Words: particle deposition, large eddy simulation

1. INTRODUCTION

Deposition of small particles or liquid droplets in turbulent boundary layers occurs in an extremely wide range of industrial and environmental applications. Examples are as diverse as deposition from paint sprays, dust inhalation, air pollution, and computer chip fabrication. In these as well as many other instances accurate prediction of the complex flow fields encountered in these systems is essential to gaining a better understanding of the phenomena governing deposition as well as ultimately improving design of the engineering devices in which two-phase flows are encountered.

Traditional methods for simulation and modeling of particle deposition in turbulent boundary layers usually rely on solution of the Reynolds-averaged Navier–Stokes (RANS) equations. The difficulty with these methods is that they rely on gradient transport hypotheses which do not accurately model particle transport, especially near the wall. This aspect of RANS methods is especially problematic for particle deposition in turbulent boundary layers. Previous work in turbulent channel flow has shown that deposition by turbulent diffusion is negligible and that the main contribution to deposition occurs through "free flight", i.e. particles becoming disengaged from fluid turbulence and gliding to the wall (Brooke *et al.* 1994).

Unfortunately, even combinations of gradient transport and free-flight models do not yield satisfactory predictions of particle deposition in turbulence. Swailes & Reeks (1994) formulated a pdf method for modeling particle deposition and applied the model to prediction of deposition in a homogeneous, stationary turbulent flow; a reasonable approximation to the deposition of high inertia particles in a boundary layer. They obtained very good agreement with the random walk model of Kallio & Reeks (1989) and also demonstrated that gradient transport and gradient transport/free-flight models were not accurate. Thus, while it is possible to resort to statistical approaches for prediction of particle deposition in turbulence, predictive techniques which are generally applicable to a wide class of flows are still needed.

The most sophisticated approach for accurately modeling particle deposition in turbulent boundary layers is direct numerical simulation (DNS). In DNS the Navier–Stokes equations are solved without approximation (other than those associated with the numerical method). DNS has

been successfully employed in a number of studies which have increased our fundamental understanding of many of the mechanisms governing deposition (e.g. see McLaughlin 1989, 1994; Brooke *et al.* 1992, 1994). These studies have shown that an accurate accounting of the underlying turbulent flows is essential for obtaining an accurate representation of particle–turbulence interactions and deposition in turbulent shear flows. The primary drawback of DNS, however, is that it remains restricted to relatively low Reynolds number flows.

An approach which is not as severely restricted in the range of Reynolds numbers as DNS is large eddy simulation (LES). In LES the large, energy-containing scales of motion are calculated directly while only the effect of the smallest (subgrid) scales of motion are modeled. Thus, LES results are less sensitive to modeling errors than in RANS calculations and, since the subgrid scales are more universal than the large scales, it is also possible to represent the effect of the subgrid scales using relatively simple models. The principal advantage of LES over RANS methods is that it permits a much more accurate accounting of particle–turbulence interactions. Since the large scales are calculated explicitly, many of the important phenomena occurring in particle-laden turbulence, e.g. accumulation of particles in low speed streaks and deposition by free flight, can be represented in LES. The principal drawback to application of LES for prediction of complex flows has traditionally been much the same as that which currently limits RANS methods, i.e. an inability of the subgrid-scale (SGS) model to account for changes in the spectral content of the turbulence under a variety of conditions, e.g. changes in the Reynolds number, type of flow, etc. without *ad hoc* tuning. The development of dynamic SGS modeling (Germano *et al.* 1991), however, has considerably improved the viability of LES as a tool for prediction of complex flows since the eddy viscosity is calculated during the course of the computation and in turn reflects local properties of the flow. SGS models which reflect local properties of the turbulence are especially attractive for computation of particle-laden flows since predictions of particle transport and deposition should be expected to be significantly improved by more accurate parameterizations of the turbulence.

Although LES and dynamic subgrid-scale models are being increasingly used in calculations of single-phase turbulent flows (e.g. see Akselvoll & Moin 1993; Squires & Piomelli 1995), they have not been widely used in the prediction of particle deposition in turbulent boundary layers. Therefore, the primary objective of this work is to use LES for prediction of particle deposition in a well-defined turbulent shear flow, fully-developed channel flow, for which DNS results and experimental measurements exist for comparison and evaluation of LES predictions (e.g. see Liu & Agarwal 1974; McCoy & Hanratty 1977; McLaughlin 1989). Both the present LES and the DNS of McLaughlin (1989) are for the deposition of particles in a vertical channel in which the forces governing particle motion are drag and shear-induced lift in the form given by Saffman (1965, 1968). Particle–particle interactions are neglected and the turbulent carrier flow is not modified by the presence of the particles.

Contained in section 2 is an overview of the simulations. Comparison of LES predictions to the DNS results of McLaughlin (1989) is presented in section 3. Because of the presence of a second phase of dispersed particles, there are additional issues relative to the calculation of deposition using LES relative to those arising in simulations of single-phase turbulence. Two of the primary issues, i.e. effect of subgrid-scale velocity fluctuations on deposition and treatment of the wall layer, are considered in section 4, including calculations of deposition which take into account SGS velocity fluctuations. A summary of the work may be found in section 5.

2. SIMULATION OVERVIEW

2.1. LES of turbulent channel flow

In LES the dependent variables are decomposed into a large scale (i.e. resolved) component and subgrid-scale contribution. The large scale variables, denoted using an overbar, are formally defined by the filtering operation:

$$\bar{f}(\mathbf{x}) = \int_D f(\mathbf{x}')\bar{G}(\mathbf{x}, \mathbf{x}')\, d\mathbf{x}', \qquad [1]$$

where D is the computational domain and $\bar{G}$ is the filter function. Application of the filtering operation to the incompressible Navier–Stokes equations yields the equations governing the motion of the resolved scales,

$$\frac{\partial \bar{u}_i}{\partial x_i} = 0, \qquad [2]$$

$$\frac{\partial \bar{u}_i}{\partial t} + \frac{\partial}{\partial x_j}(\bar{u}_i \bar{u}_j) = -\frac{\partial \bar{p}}{\partial x_i} + \frac{1}{\mathrm{Re}_\tau}\frac{\partial^2 \bar{u}_i}{\partial x_j \partial x_j} - \frac{\partial \tau_{ij}}{\partial x_j}. \qquad [3]$$

Note that the filtered equations of motion have been made dimensionless using the friction velocity u_τ and channel half-width δ. The Reynolds number appearing in [3] is then $\mathrm{Re}_\tau = u_\tau \delta / \nu$, where ν is the kinematic viscosity. The velocity components $\bar{u}_i$ for $i = 1$, 2 and 3 refer to the streamwise (x), wall-normal (y), and spanwise directions (z), respectively (the usual summation notation applies).

The effect of the small scales on the large energy-containing eddies in [3] is represented by the SGS stress, $\tau_{ij} = \overline{u_i u_j} + \bar{u}_i \bar{u}_j$. In this as well as the majority of LES work τ_{ij} is parameterized using an eddy viscosity hypothesis,

$$\tau_{ij} - \tfrac{1}{3}\delta_{ij}\tau_{kk} = -2\nu_T \bar{S}_{ij}, \qquad [4]$$

where the eddy viscosity is defined as $\nu_T = C\bar{\Delta}^2 |\bar{S}|$. The resolved-scale strain rate tensor is

$$\bar{S}_{ij} = \frac{1}{2}\left(\frac{\partial \bar{u}_i}{\partial x_j} + \frac{\partial \bar{u}_j}{\partial x_i}\right), \qquad [5]$$

and $|\bar{S}| = \sqrt{2\bar{S}_{ij}\bar{S}_{ij}}$ is the magnitude of $\bar{S}_{ij}$. The filter width is $\bar{\Delta} = (\bar{\Delta}_x \bar{\Delta}_y \bar{\Delta}_z)^{1/3}$ where $\bar{\Delta}_x$, $\bar{\Delta}_y$, and $\bar{\Delta}_z$ are the grid spacings in the x, y and z directions, respectively. The model coefficient C requires specification in order to close the system [2] and [3].

In this study the dynamic approach developed by Germano *et al.* (1991) was used to calculate C. The philosophy of dynamic modeling is to take advantage of information available in LES and calculate the model coefficient during the course of the simulation using information from the resolved scales. In dynamic modeling a second filter, referred to as the test filter and denoted using $\hat{}$, is introduced. The test filter is defined at a slightly larger scale than the grid filter and is therefore applied to a more narrow range of scales. One can define a test filtering operation analogous to [1] and application of the test filter to [2] and [3] will yield the equations governing the test-filtered variables. This procedure will in turn yield a subtest-scale stress, $T_{ij} = \widehat{\bar{u}_i \bar{u}_j} - \hat{\bar{u}}_i \hat{\bar{u}}_j$. Germano (1992) showed that the relation between τ_{ij}, T_{ij}, and the resolved turbulent stress $\mathscr{L}_{ij} = \widehat{\bar{u}_i \bar{u}_j} - \hat{\bar{u}}_i \hat{\bar{u}}_j$ is

$$\mathscr{L}_{ij} = T_{ij} - \hat{\tau}_{ij}. \qquad [6]$$

In Germano *et al.* (1991), [4] and an analogous expression for T_{ij} are substituted into [6]. Lilly (1992) used a least-squares approach to solve the resulting system of equations for the model coefficient C:

$$C(y,t) = -\frac{1}{2}\frac{\langle \mathscr{L}_{ij} M_{ij} \rangle_{xz}}{\langle M_{kl} M_{kl} \rangle_{xz}}, \qquad [7]$$

where

$$M_{ij} = \hat{\bar{\Delta}}^2 |\hat{\bar{S}}| \hat{\bar{S}}_{ij} - \bar{\Delta}^2 \widehat{|\bar{S}| \bar{S}_{ij}}. \qquad [8]$$

In [7], $\langle\rangle_{xz}$ denotes averaging over x–z planes in the channel. Averaging the numerator and denominator of [7] are required in order to avoid large local variations in C as well as negative values which cause numerical instability. Thus, as shown in [7] the coefficient is a function of distance from the wall and time (see Piomelli & Liu 1994; Ghosal *et al.* 1994, and Meneveau *et al.* 1994 for further discussion). The only parameter needed to be specified in the dynamic model is the ratio between the test filter width, $\hat{\bar{\Delta}}$, and grid scale filter width $\bar{\Delta}$. As has been shown by Germano *et al.* (1991), LES results are not overly sensitive to this ratio and in this study $\hat{\bar{\Delta}}/\bar{\Delta} = 2^{2/3}$. Test filtering in the streamwise and spanwise directions was carried out in Fourier space using a sharp cut-off filter.

The filtered equations of motion [2] and [3] will allow one to obtain representations of the large scales which are statistically similar to DNS results or experimental measurements. A single realization of an LES calculation, however, will differ from a DNS or experiment due to errors which arise in the LES due to the subgrid model. However, since τ_{ij} models only the effect of the unresolved scales and the dominant nonlinear transfer is from large to small scales, the large-scale statistics should not be unduly influenced by errors in the SGS model.

The governing equations [2] and [3] were solved numerically using the fractional step method (e.g. see Kim & Moin 1985; Perot 1993; Wu *et al.* 1995). Spatial derivatives were expressed using second-order accurate central differences on a fully staggered grid. The continuity equation [2] was enforced about the pressure nodes in each cell and the momentum equation [3] was satisfied about the velocity nodes. To avoid the stability restriction imposed by the viscous terms an implicit time advance scheme was applied. The second-order Adams–Bashforth method was used for advancement of the convective terms and part of the SGS term while the Crank–Nicholson method was applied for update of the viscous terms and a portion of the SGS stress. The Poisson equation for pressure was solved using series expansions in the streamwise and spanwise directions together with tridiagonal matrix inversion (e.g. see Williams 1969; Kim & Moin 1985).

Experimental measurements of particle deposition in turbulent flows have shown that, when scaled in wall units, the deposition rate is well correlated with the square of the particle relaxation time for particles with time constants τ^+ varying from about 0.2 to 23 (Liu & Agarwal 1974; McCoy & Hanratty 1977). This feature was examined in the present work using calculations performed at two Reynolds numbers, Re_τ, of 180 and 1000 (based on friction velocity and channel half width). The corresponding Reynolds numbers based on centerline velocity are 3200 and 21,900, respectively. Those defined using the bulk velocity and hydraulic diameter are 11,160 and 79,400, close to the Reynolds numbers of 10,000 and 50,000 in the experiments of Liu & Agarwal (1974). The filtered equations were discretized using $64 \times 65 \times 64$ grid points (65 points in the wall-normal direction). The channel domain for the calculations performed at $\mathrm{Re}_\tau = 180$ was $4\pi\delta \times 2\delta \times 4\pi\delta/3$ and $5\pi\delta/2 \times 2\delta \times \pi\delta/2$ for the simulations performed at $\mathrm{Re}_\tau = 1000$. The spatial resolution in wall coordinates in the streamwise and spanwise directions was $\Delta x^+ = 35$ and $\Delta z^+ = 12$ at $\mathrm{Re}_\tau = 180$ and $\Delta x^+ = 123$ and $\Delta z^+ = 25$ at $\mathrm{Re}_\tau = 1000$. For the moderate Reynolds numbers considered in this work the wall-normal direction is resolved, i.e. the first grid point away from the wall was located at $y^+ = 0.45$ and $y^+ = 0.9$ for the calculations at $\mathrm{Re}_\tau = 180$ and 1000, respectively. At substantially higher Reynolds numbers direct resolution of the wall is not economical and different approaches will be required for simulation and modeling of particle deposition (see section 4 for further discussion).

2.2. *Calculation of particle trajectories*

The particle equation of motion employed in the calculations is similar to that used by McLaughlin (1989) and is appropriate for describing the motion of particles with densities substantially larger than the surrounding fluid and diameters smaller than the Kolmogorov lengthscale:

$$\frac{\mathrm{d}v_i}{\mathrm{d}t} = -\frac{\rho_\mathrm{f}}{\rho_\mathrm{p}}\frac{3}{4}\frac{C_D}{d}|\mathbf{v}-\mathbf{u}|(v_i-u_i)+f_i. \qquad [9]$$

In [9] v_i is the particle velocity, u_i is the velocity of the fluid at the particle position, and f_i is the lift force per unit mass (directed in the wall-normal direction, i.e. $f_1 = f_3 = 0$). The fluid and particle densities in [9] are denoted ρ_f and ρ_p, respectively, and d is the particle diameter. Previous computations have shown that for particles which deposit the particle Reynolds number, $\mathrm{Re}_\mathrm{p} = d|\mathbf{u}-\mathbf{v}|/\nu$, does not necessarily remain small (McLaughlin 1989). Therefore, an empirical relation given by Clift *et al.* (1978) was used to account for effects of nonlinear drag:

$$C_D = \frac{24}{\mathrm{Re}_\mathrm{p}}[1 + 0.15\mathrm{Re}_\mathrm{p}^{0.687}]. \qquad [10]$$

The calculations correspond to a vertical channel in which gravity does not directly lead to deposition and therefore its effect has not been included in [9]. Neglect of gravitational drift also facilitates comparison with the DNS results of McLaughlin (1989) in which gravity was neglected.

The form of shear-induced lift in [9] is the same as in McLaughlin (1989) and was derived by Saffman (1965, 1968),

$$f_i = \frac{F_i}{\frac{4}{3}\pi(a\delta)^3\rho_p}\frac{1}{u_\tau^2/\delta} = -\frac{0.343a}{\tau}(v_1 - u_1)\frac{du_1/dy}{|du_1/dy|}\left[\frac{1}{Re_\tau}\left|\frac{du_1}{dy}\right|\right]^{1/2}\delta_{i2}, \quad [11]$$

where F_i is the dimensional lift force acting on the particle, a is the particle radius, τ is the Stokes time constant, and δ_{ij} is the Kronecker delta. It should also be noted that the influence of virtual mass, buoyancy, and the Basset history force on particle motion are neglected in [9]. For particles with material densities large compared to the fluid these forces are negligible compared to the drag. More importantly, however, [9] does not account for effects of the wall on particle motion nor particle–particle interactions. Modification of the forces on a particle by these effects could have a significant influence on motion very near the wall (e.g. see Chen *et al.* 1995).

From computation of an Eulerian velocity field as described in section 2.1, [9] was integrated in time using the second-order Adams–Bashforth method. For particles that moved out of the channel in the streamwise or spanwise directions periodic boundary conditions were used to reintroduce it in the computational domain. Deposition was assumed to occur when a particle was within one radius of the wall. Since it is only by chance that a particle is located at a grid point where the velocity field is available, interpolation is required in order to determine the fluid velocity at the particle position. Previous calculations of homogeneous turbulence and turbulent channel flow (e.g. Yeung & Pope 1988; Balachandar & Maxey 1989; Kontomaris *et al.* 1992) have shown statistical quantities acquired along particle trajectories are sensitive to the interpolation scheme. Fourth-order Lagrange polynomials were used to obtain fluid velocities at particle positions (see the appendix for further discussion).

In the majority of cases considered in this work the particle velocity is driven by the resolved fluid velocity in [9], i.e. the contribution of subgrid scale velocity fluctuations has been neglected. Neglect of particle transport by subgrid scale velocities is a source of error in the simulations and should be expected to be more significant for particles with smaller relaxation times, i.e. for particles more responsive to subgrid scale motions occurring on smaller timescales. The reader is referred to section 4 for additional discussion of the effect of the subgrid-scale velocity field on deposition.

3. RESULTS

The principal focus of this section is comparison of LES predictions to the DNS results of McLaughlin (1989). Therefore, properties of particle deposition from LES at $Re_\tau = 180$ are presented for the same particle relaxation times and density ratios as used by McLaughlin (1989). For each time constant 20,000 particles were used in the simulations. The initial locations of the particles were chosen randomly and the particle velocity was initially identical to that of the fluid at the particle position. The particle relaxation time is expressed in wall units as $\tau^+ = 2\rho a^{+2}/9$ where $\rho = \rho_p/\rho_f$. McLaughlin (1989) considered $2 \leqslant \tau^+ \leqslant 6$ and density ratios of 713, 1500 and ∞. The corresponding variation in the particle radius a^+ is 0.11–0.19 for $\rho = 713$ and 0.08–0.13 for $\rho = 1500$. Thus, very near the wall the particle diameter can be comparable to the wall-normal grid spacing and the effect of a nonuniform fluid velocity field on particle motion may be less accurately represented.

Shown in figure 1 is the wall-normal profile of the particle concentration. The results shown in figure 1 were obtained after $1.5\delta/u_\tau$ (270 viscous units) for particles with $\rho = 713$, $\tau^+ = 6$ and $\rho = \infty$ (corresponding to $f_2 = 0$), $\tau^+ = 2$. Figure 1 clearly shows that the particle distribution peaks at or near the wall and the effect is much more pronounced for the larger relaxation time. Comparison with the initial distribution in figure 1 does in fact indicate that particles with $\tau^+ = 2$ exhibit larger concentrations near the wall. This result from the present LES is similar to that previously demonstrated by McLaughlin (1989) that there is an accumulation of particles in the near-wall region; the accumulation being stronger for particles with larger relaxation time (see also Brooke *et al.* 1992, 1994; Rouson & Eaton 1994). For simulations performed with particles having $\rho = 713$, $\tau^+ = 6$ the peak concentration is about 7 times larger than for a random distribution while the peak concentration is about 1.5 times larger for particles with $\rho = \infty$ and $\tau^+ = 6$ at $t = 1.5$.

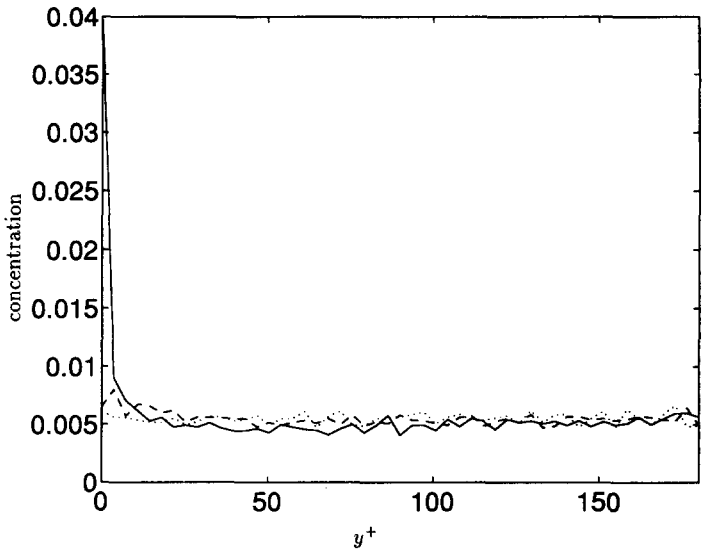

Figure 1. Particle concentration, $\mathrm{Re}_\tau = 180$. $\rho = 713$, $\tau^+ = 6$: $\cdots$ $t = 0$; ——$t = 1.5$; $\rho = \infty$, $\tau^+ = 2$: $\cdots$ $t = 0$; – – – $t = 1.5$.

The average Saffman lift force and normal component of the drag force on particles that deposit are shown in figure 2. The forces have been averaged over both walls of the channel by reversing the signs of the forces for particles which deposited on the upper wall. It may be observed from figure 2 that LES predictions are in reasonable agreement with the DNS results of McLaughlin (1989); the magnitude and location of the peaks of the forces being reasonably well predicted. For increasing particle relaxation times both lift and wall-normal drag forces are reduced relative to the values for particles with smaller τ^+. As may be observed from the figure, the reduction in the lift force with increasing τ^+ is less than the change observed in the wall-normal drag, consistent with the dependence of the drag on $1/\tau$ and lift on $1/\sqrt{\tau}$. It is also apparent in figure 2 that the drag force for $\tau^+ = 20$ and 40 does not change sign as observed for particles with smaller τ^+ since, near the wall, particles with large relaxation times have increasingly larger wall-normal velocities than the fluid (c.f. figure 4). Consistent with McLaughlin (1989) as well as Kallio & Reeks (1989),

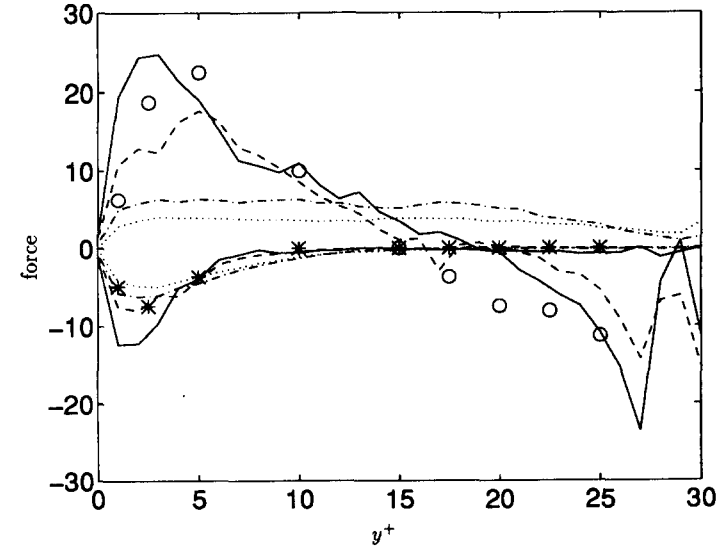

Figure 2. Saffman lift force and wall-normal component of drag averaged over particles that deposit, $\rho = 713$, $\mathrm{Re}_\tau = 180$. Upper curves (near $y^+ = 0$) are the drag; lower curves are the lift. LES: $\tau^+ = 3$: ——; $\tau^+ = 4$: – – –; $\tau^+ = 20$: — · —; $\tau^+ = 40$: $\cdots$; McLaughlin (1989) ($\tau^+ = 3$): ○ drag force; * lift force.

the figure also shows that the lift force is active only in the viscous sublayer. As also shown by McLaughlin (1989), though the Saffman lift is small relative to the drag force, the impulse imparted to particles is sufficient to cause deposition.

The ratio of the average wall-normal component of the fluid velocity at the location of deposited particles to the intensity of the wall-normal fluctuations is shown in figure 3. Figure 3 shows that the greatest discrepancy between LES predictions and DNS results is in the behavior for particles with $\tau^+ = 2$. The large eddy simulation shows a rapid decrease in the ratio for y^+ between 5 and 10 while the DNS results shows a more gradual decrease; the peak in the LES predictions is also nearer the wall than in the DNS calculation. Differences between the LES and DNS arise from both errors in prediction of the large scales by LES as well as lack of sample of particles over which the statistics presented in figure 3 were averaged. The results in figure 3 show that LES is capable of accounting for the fact that the wall-normal velocity of particles which deposit is substantially larger than the wall-normal turbulence intensity and demonstrates the influence of free flight (see Brooke *et al.* 1994 for a detailed discussion).

Shown in figure 4 is the relative velocity averaged over deposited particles. In comparison with McLaughlin (1989), LES predictions yield approximately the same magnitude and signs in the relative velocities for both the streamwise and wall-normal components as well as the location of the maximum values. However, it may also be observed that LES predictions for particles with $\tau^+ = 4$ are in slightly better agreement with DNS results for $\tau^+ = 3$ than are the LES predictions for the same relaxation time. Differences in the streamwise component of the slip velocity are probably related to the over-prediction of streamwise intensities in the LES calculation. As pointed out by McLaughlin (1989), it is the large difference in streamwise velocities between particles and fluid which lead to relatively large Reynolds numbers of depositing particles. In the present study the particle Reynolds number for particles with $\tau^+ = 6$ has a maximum value of 0.2 when averaged over all particles in the channel. The maximum Reynolds number of particles which deposit was found to be about 0.9. Both LES and DNS results clearly show that the streamwise velocity difference is much larger than the wall-normal relative velocity. More importantly, similar to the DNS, LES predictions also show that near the wall particles lead/lag the fluid in the streamwise/wall-normal direction but this behavior is reversed for y^+ greater than approximately 12–15. It may also be seen in figure 4 that for increasing values of the particle relaxation time the relative velocities in both the streamwise and wall-normal directions increase, consistent with the fact that particles with small τ^+ track the flow more closely.

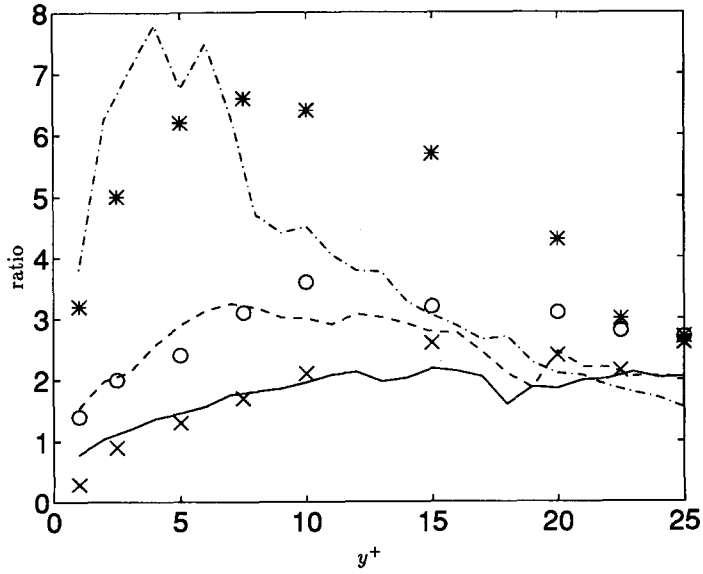

Figure 3. Ratio of wall-normal component of averaged fluid velocity at the location of deposited particles to wall-normal turbulence intensity, $\rho = 713$, $Re_\tau = 180$. LES: —·— $\tau^+ = 2$; – – – $\tau^+ = 4$; —— $\tau^+ = 6$; McLaughlin (1989): * $\tau^+ = 2$; ○ $\tau^+ = 4$; x $\tau^+ = 6$.

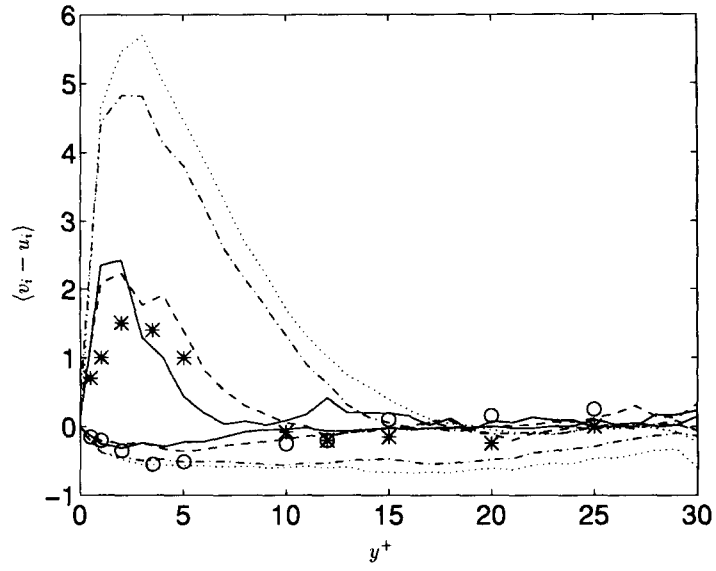

Figure 4. Relative velocity averaged over particles that deposit, $\rho = 713$, $Re_\tau = 180$. Upper curves (near $y^+ = 0$) are the streamwise velocity difference; lower curves are the wall-normal velocity difference. LES: $\tau^+ = 3$: ——; $\tau^+ = 4$: – – –; $\tau^+ = 20$: — · —; $\tau^+ = 40$: · · ·; McLaughlin (1989) ($\tau^+ = 3$): ○ wall normal; * streamwise.

Correlation coefficients between the wall-normal components of the fluid and particle velocities are shown in figure 5. In general, the agreement between LES predictions and DNS is best for particles with larger relaxation times. Particle motion for large τ^+ is mostly influenced by the largest scales of motion, i.e. eddies with timescales comparable to the particle. The largest eddies are accurately represented in LES, i.e. less affected by errors in the subgrid model. On the contrary, particles with smaller relaxation times are responsive to a broader spectrum of scales. Errors in representation of the smallest resolved scales and SGS motions will adversely affect prediction of particle motion. However, even for $\tau^+ = 2$ it may be observed in figure 5 that LES predictions of the correlation between particle and fluid velocities is satisfactory. Figure 5 also shows that the

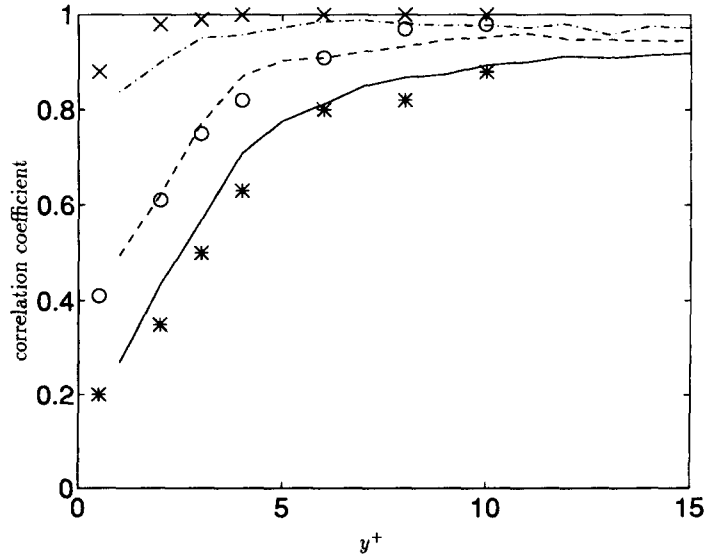

Figure 5. Correlation coefficient of the particle velocity and fluid velocity at particle position for the particles that deposit, $\rho = 713$, $Re_\tau = 180$. LES: — · — $\tau^+ = 2$; – – – $\tau^+ = 4$; —— $\tau^+ = 6$; McLaughlin (1989): x $\tau^+ = 2$; ○ $\tau^+ = 4$; * $\tau^+ = 6$.

correlation coefficients between the wall-normal particle and fluid velocities for the depositing particles are much smaller than unity near the wall, especially for particles with large relaxation times. This result again demonstrates that particles are brought to the near-wall region by turbulent motions but travel to the wall (i.e. deposit) by free flight.

Additional comparison of LES predictions to experimental measurements and DNS results is obtained through examination of the particle deposition rate (also known as the deposition velocity). The deposition rate is defined as the ratio of the flux of particles at the deposition surface to the particle concentration (i.e. the number of particles per unit volume). For a deposition of N_d particles on the wall from a total number N in a time interval t, the deposition rate is then

$$V_d = \frac{N_d/A/t}{N/V}, \qquad [12]$$

where A is the area of the deposition surface and V is the volume of the computational domain.

The particle deposition rate for the same density ratios and particle relaxation times as in the DNS study by McLaughlin (1989) is presented in figure 6. Also shown in the figure is the empirical expression from Liu & Agarwal (1974). For the range of τ^+ shown in the figure sampling intervals greater than 600 wall units were sufficient for obtaining deposition velocities which were converged, i.e. increases in the sampling interval did not appreciably change the deposition rate. As can be seen from figure 6, LES predictions exhibit the same dependence on relaxation time and density ratio as in DNS but are below the results of McLaughlin (1989). The particle deposition rate increases for increasing particle relaxation times and decreasing density ratios. Since $\rho = \infty$ corresponds to dropping the lift term from the particle equation of motion, it is evident from the figure that the Saffman lift force increases particle deposition. It should also be noted that, for fixed τ^+, the interception length decreases with increasing density ratio and this can also lead to a reduction in deposition. It is also clear from figure 6 that both the LES and DNS calculations yield deposition rates which are in fair agreement with those obtained from the empirical relation of Liu & Agarwal (1974). However, experimental measurements suggest that the deposition rate increases quadratically with particle relaxation time whereas figure 6 shows that both LES and DNS predict a dependence larger than τ^{+2}.

The specific dependence of the deposition rate on relaxation time and scaling in inner variables was investigated through LES of channel flows at a higher Reynolds number than previously considered, i.e. $Re_\tau = 1000$, and for a wider range of particle relaxation times. The deposition rate

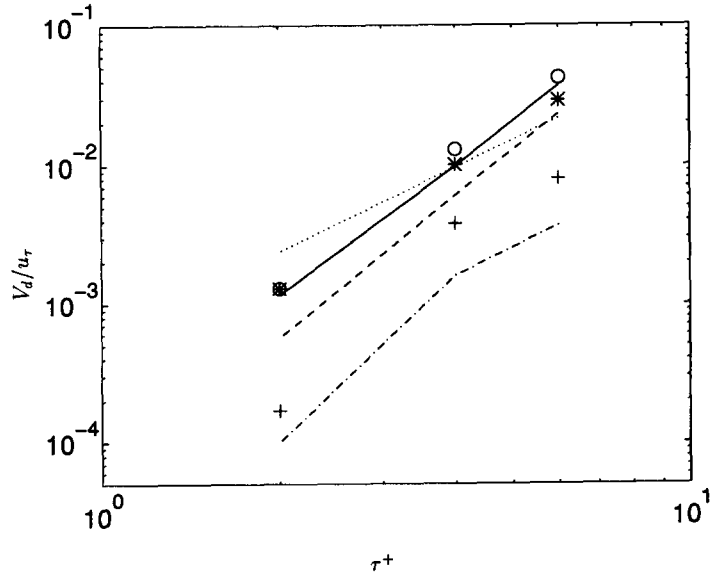

Figure 6. Particle deposition rate in turbulent channel flow, $\cdots$ $V_d = 0.0006\tau^{+2}$ (Liu & Agarwal 1974); LES: —— $\rho = 713$; - - - $\rho = 1500$; — · — $\rho = \infty$ McLaughlin (1989): ○ $\rho = 713$; * $\rho = 1500$; + $\rho = \infty$.

as a function of the particle relaxation time is shown in figure 7 for $\rho = 713$, corresponding to the deposition of olive oil droplets in air and considered in the experiments of Liu & Agarwal (1974). Also shown in figure 7 are the experimental measurements of Liu & Agarwal (1974) together with their empirical relation as well as that from McCoy & Hanratty (1977). It is evident from figure 7 that the deposition rates obtained at the two Reynolds numbers are nearly the same, implying that the LES properly reflects the scaling of the deposition velocity with relaxation time. The magnitudes of the deposition rate agree well with the experimental measurements for $\tau^+ > 3$. However, the deposition rate for smaller relaxation times is less than the experimentally measured values. For small τ^+ it is difficult to obtain accurate values of the deposition rate since there are fewer depositing particles in these simulations. It is further difficult to obtain precise estimates of the uncertainty in calculation of the deposition rate since performance of several simulations from which one could ensemble average is prohibitively expensive.

A least-squares fit of the LES predictions yields a dependence of the deposition rate on particle relaxation time of $\tau^{+2.72}$ which is substantially larger than the quadratic dependence observed experimentally. It should also be noted that for the largest relaxation time in the calculation, $\tau^+ = 200$, the maximum value of Re_p is 4.5 when averaged over all particles; for the depositing particles the Reynolds number is even larger. Thus, for increasing values of τ^+ application of the Saffman formula is questionable and LES predictions for the largest relaxation times must therefore be treated with caution. However, it is interesting to note that figure 7 shows the deposition rate becomes roughly independent of particle relaxation time for large τ^+ and is in reasonable agreement with experimentally measured values.

4. EFFECT OF SGS FLUCTUATIONS AND TREATMENT OF THE WALL

In LES the smallest scales of motion are not resolved by the computational grid, only their effect on the large eddies is represented via the SGS model. Thus, when considering particle

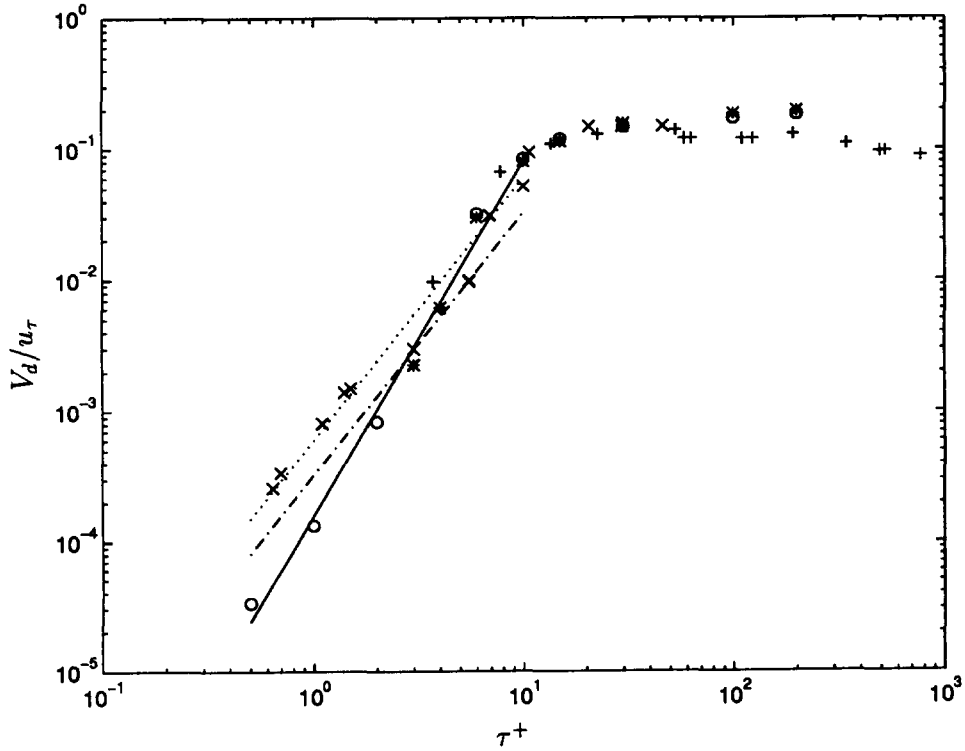

Figure 7. Particle deposition rate in turbulent channel flow, LES calculations performed using Saffman lift force, $\rho = 713$. $\cdots$ $V_d = 0.0006\tau^{+2}$ (Liu & Agarwal 1974); —·— $V_d = 0.000325\tau^{+2}$ (McCoy & Hanratty 1977). LES: ○ $Re_\tau = 180$; * $Re_\tau = 1000$; —— least-squares fit of LES results; Liu & Argarwal (1974) (Reynolds numbers based on pipe diameter and average velocity): x Re = 10,000; + Re = 50,000.

transport and deposition only the large-scale velocity fluctuations are directly available in an LES computation for determining particle motion. For the results presented in the previous section the effect of subgrid-scale velocity fluctuations on particle deposition were neglected. This should be a justifiable assumption in most applications in which particles with material densities large compared to the carrier flow are being considered. In the absence of a mean flow the response of particles to the frequency spectrum of the turbulence can be shown to be proportional to $1/(\tau\omega)^2$ (ω is the frequency). Thus, for increasing values of the relaxation time and/or frequency the filtering of high frequency motions by particle inertia is significant.

Nevertheless, one source of error in LES predictions of particle deposition will be due to the neglect of transport by SGS turbulence. A measure relevant to this error is comparison of the smallest resolved timescale in the LES to the particle relaxation time. Shown in figure 8 is the wall-normal profile of the smallest resolved timescale defined in terms of the filter width $\bar{\Delta}$ and velocity scale used in specification of the eddy viscosity $\bar{\Delta}|\bar{S}|$, i.e. $T = 1/|\bar{S}|$. The timescale shown in the figure (in wall units) is from calculations performed at $\mathrm{Re}_\tau = 180$ and it may be observed that T^+ increases from about two very near the wall to roughly 20 near the channel centerline. Thus, T^+ is comparable to the particle relaxation times considered in the calculations presented in section 3 and it is therefore possible that SGS velocity fluctuations may have a measurable effect on deposition, especially for small τ^+. Therefore, the effect of SGS velocity fluctuations on deposition was examined by modeling the subgrid-scale velocity field and including SGS fluctuations in the particle equation of motion [9].

Calculations were performed in which the fluid velocity in the particle equation of motion was the resolved component $\bar{u}_i$, directly available in the LES, plus a subgrid component u_i'. The magnitude of the SGS fluctuation u_i' was determined by solving an additional transport equation for SGS kinetic energy, q^2. The transport equation used for determination of q^2 is that proposed by Schumann (1991), i.e.

$$\frac{\partial q^2}{\partial t} + \bar{u}_j \frac{\partial q^2}{\partial x_j} = 2\nu_T |\bar{S}|^2 + \frac{\partial}{\partial x_j}\left(\tfrac{1}{3} l_\Delta \sqrt{q^2/2}\, \frac{\partial q^2}{\partial x_j}\right) + \nu \frac{\partial^2 q^2}{\partial x_j \partial x_j} - \sqrt{\tfrac{1}{2}} c_\epsilon \frac{q^3}{l_\Delta}, \qquad [13]$$

where

$$c_\epsilon = \pi \left(\frac{2}{3k_0}\right)^{3/2}, \quad l_\Delta = \min\{\bar{\Delta}, c_\epsilon y\}, \qquad [14]$$

with the Kolmogorov constant $k_0 = 1.6$.

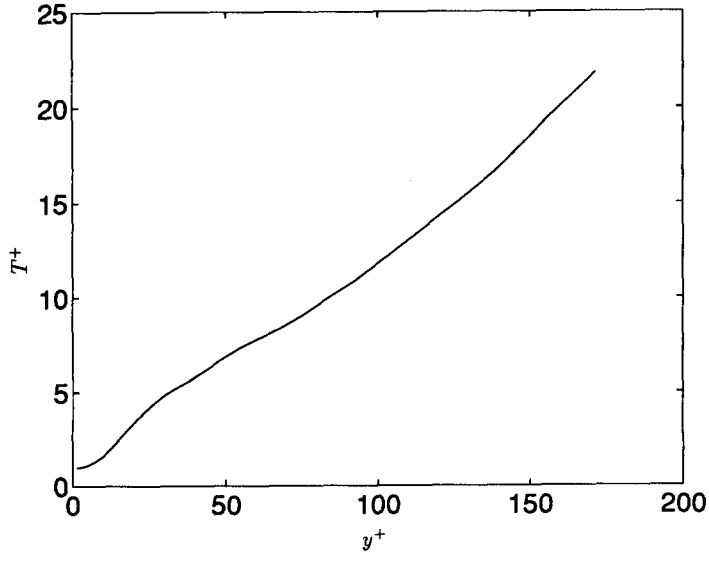

Figure 8. Smallest resolved timescale, $\mathrm{Re}_\tau = 180$.

Solution of [13] yields the magnitude of the SGS kinetic energy throughout the channel. The SGS components $u_i'^2$ were then obtained from q^2 and specified to have the same relative magnitudes as the resolved-scale intensities. The component fluctuations u_i' were then scaled by random numbers sampled from a Gaussian distribution and added to $\bar{u}_i$ at the particle location. The complete velocity, i.e. $\bar{u}_i + u_i'$, was used in [9] to determine the particle velocity.

Figure 9 shows the effect of SGS velocity fluctuations on the lift force and wall-normal component of the drag averaged over particles that deposit. Profiles are shown for $\tau^+ = 4$ and it is clear that the difference between the forces in simulations in which SGS velocities are included is small relative to results obtained with no SGS velocities. The effect of SGS fluctuations on the ratio of the wall-normal component of averaged fluid velocity for deposited particles to wall-normal turbulence intensity is shown in figure 10. The figure shows that for particles with $\tau^+ = 6$, there is virtually no effect of SGS velocities while for $\tau^+ = 2$ subgrid-scale fluctuations increase the wall-normal velocities for depositing particles by 30% near $y^+ = 5$. This result is consistent with the arguments made previously in that effects of SGS fluctuations should be more pronounced for smaller τ^+ since these particles are more responsive to a broader range of frequencies of turbulent velocities. Predictions of the particle deposition rate with and without SGS velocities are compared in figure 11. The figure again demonstrates the greatest effect of SGS fluctuations occurs for the smallest particle relaxation times. As may be observed in the figure, inclusion of SGS velocity fluctuations changes the deposition rate but the difference in predictions with and without SGS velocities is relatively small, e.g. less than 10% for $\tau^+ = 2$ and $\rho = 1500$.

The figures shown above are representative samples of the effect of SGS fluctuations on particle deposition. It is important to note that the effect of the subgrid scale fluctuations on deposition will be dependent upon the Reynolds number or, equivalently, the resolution used in the LES. For a fixed geometry and grid size, increases in the Reynolds number will correspond to an increasing fraction of turbulence energy residing in the subgrid scales and a greater effect of small-scale fluctuations on particle motion. In this work a turbulent channel flow at relatively low Reynolds number was considered in order to facilitate comparison to the DNS results from McLaughlin (1989). At higher Reynolds number, i.e. coarser resolution, the effect of SGS turbulence will be more pronounced.

Another aspect of the current simulations, and common to the majority of LES calculations currently performed, is that the wall-normal resolution is relatively fine. Fine resolution is necessarily required in order to adequately capture mean-flow gradients in simulations in which the first grid point is located on the wall. At substantially higher Reynolds numbers, however,

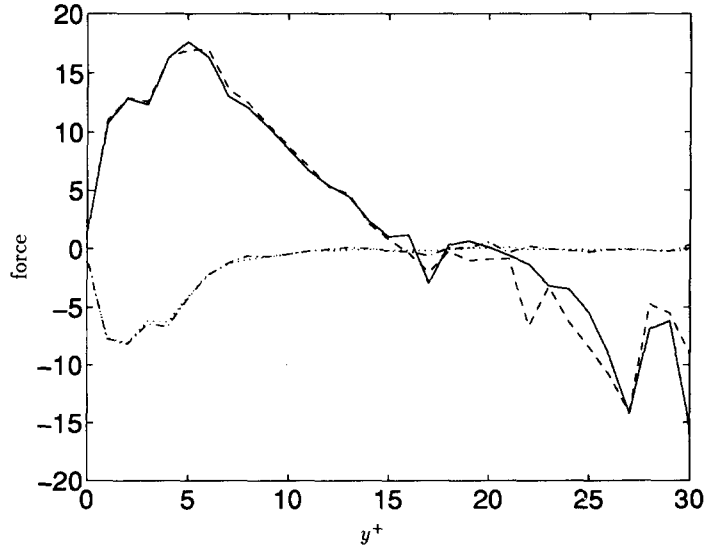

Figure 9. Effect of SGS velocity fluctuations on Saffman lift force and wall-normal component of drag averaged over particles that deposit, $\rho = 713$, $\tau^+ = 4$, $Re_\tau = 180$. No SGS velocity: —— drag force; ··· lift force; including SGS velocity: – – – drag force; —·— lift force.

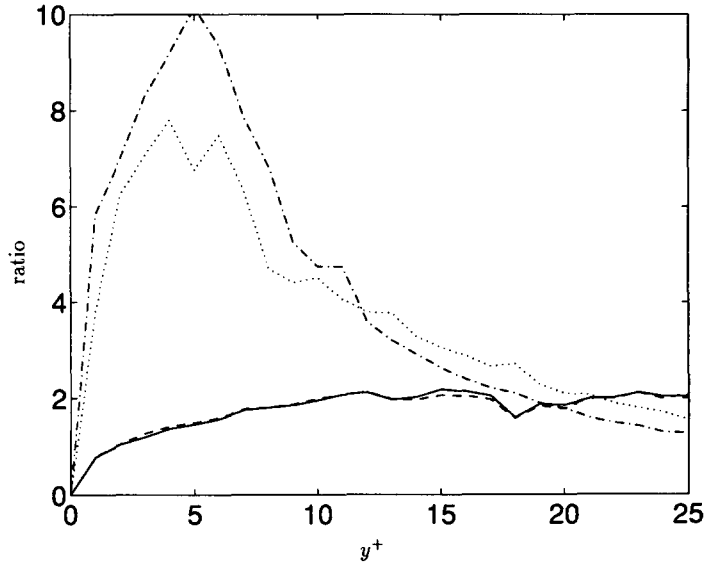

Figure 10. Effect of SGS velocity fluctuations on the ratio of wall-normal component of averaged fluid velocity for particles that deposit to wall-normal turbulence intensity, $\rho = 713$, $Re_\tau = 180$. No SGS velocity: $\cdots$ $\tau^+ = 2$; —— $\tau^+ = 6$; including SGS velocity: — · — $\tau^+ = 2$. – – – $\tau^+ = 6$.

location of the first grid point on the wall becomes increasingly expensive. In LES of single-phase flows the restrictive requirements imposed by high Reynolds numbers are circumvented through the use of approximate boundary conditions. It is assumed that the dynamics of the wall layer are universal and some form of a generalized law of the wall can be imposed (e.g. see Schumann 1975). The first grid point is then located away from the wall and boundary conditions consistent with a desired property of the flow are enforced, e.g. a logarithmic layer.

It should be possible to use an extension of this approach to predict particle deposition in high Reynolds number LES provided that approximate boundary conditions are available for a particular flow field, e.g. pipes and channels. One approach is illustrated schematically in figure 12. Shown in the figure is the near-wall region of a turbulent boundary layer in which, for the sake of discussion, approximate boundary conditions are applied in an LES calculation at $y^+ = 200$. For larger values of y^+ the filtered Navier–Stokes equations are solved to obtain a description of the large-scale velocity field. Particle motion in the outer flow is then responsive to the large eddies

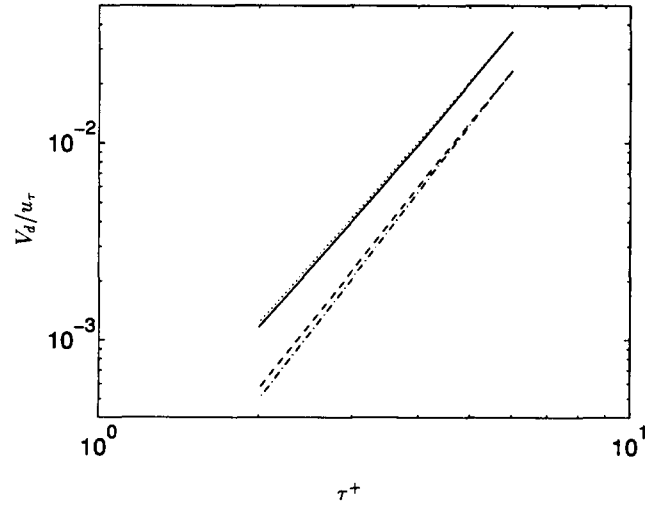

Figure 11. Effect of SGS velocity fluctuations on particle deposition rate in turbulent channel flow. No SGS velocity: —— $\rho = 713$; – – – $\rho = 1500$; including SGS velocity: $\cdots$ $\rho = 713$; — · — $\rho = 1500$.

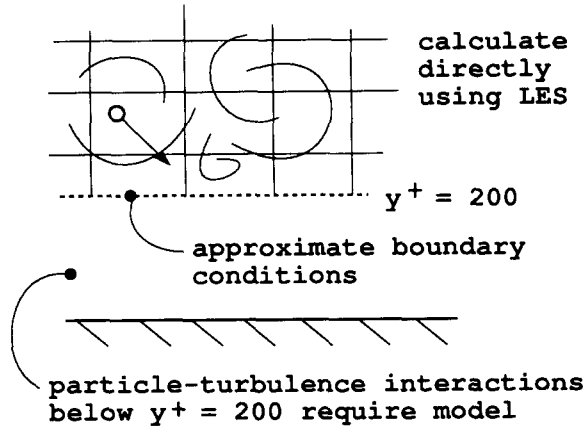

Figure 12. A possible approach for calculating deposition at high Reynolds numbers in which the outer flow ($y^+ > 200$) is calculated using LES. Approximate boundary conditions are applied at $y^+ = 200$; stochastic models used to account for particle–turbulence interactions below $y^+ = 200$.

(and possibly the SGS velocities using a scheme similar to that described above). As a particle moves across the plane $y^+ = 200$ only the mean velocity is available via the approximate boundary conditions, e.g. the law of the wall. Particle response to turbulent motions requires a model. In this region random walk/random flight models may provide a feasible method for modeling particle response to turbulence and calculating deposition. The random walk model of Kallio & Reeks (1989) provides one such example. Further, the wealth of information extracted from DNS (e.g. see Brooke *et al.* 1994) will also be useful for model development.

5. SUMMARY

Results obtained in this work indicate that LES is a viable approach for predicting particle deposition in turbulent boundary layers. LES predictions were found to be in reasonable agreement with the DNS results of McLaughlin (1989). Though LES predictions of particle deposition rates are in relatively good agreement with McLaughlin (1989), the values obtained in both LES and DNS are below experimental measurements. Including effects such as particle collisions will further improve agreement between simulation and experiment since Chen *et al.* (1995) have recently shown deposition rates are increased by accounting for particle-particle interactions.

In general, the greatest discrepancy between LES and DNS occurs for particles possessing the smallest relaxation times. Since particles with small τ^+ are responsive to a relatively broad spectrum of turbulent motions, neglect of subgrid-scale velocity fluctuations is a source of error in the use of LES for calculation of particle transport in turbulence. However, using a relatively simple approach for representation of SGS velocities, it was shown that SGS velocity fluctuations did not have a large effect on deposition. At substantially higher Reynolds numbers, however, incorporation of SGS fluctuations may be important, especially for statistics involving wall-normal fluctuations. Furthermore, for very high Reynolds numbers in which approximate boundary conditions are used in the LES, treatment of the near-wall region becomes more complex since LES can be used to model particle–turbulence interactions only in the outer flow. Application of LES in conjunction with models of particle transport very near the wall comprise an important direction for future research.

Acknowledgements—This work is supported by the National Institute of Occupational Safety and Health (Grant Number OH03052-02). Computer time for the simulations was supplied by the Cornell Theory Center.

REFERENCES

Akselvoll, K. & Moin, P. 1993 Application of the dynamic localization model to large-eddy simulation of turbulent flow over a backward facing step. *Engineering Applications of Large Eddy Simulation* (Edited by S. Ragab & U. Piomelli), ASME FED, Vol. 162, pp. 1–6.

Balachandar, S. & Maxey, M. R. 1989 Method for evaluating fluid velocities in spectral simulation of turbulence. *J. Comput. Phys.* **83,** 96–125.

Brooke, J. W., Kontomaris, K., Hanratty, T. J. & McLaughlin, J. B. 1992 Turbulent deposition and trapping of aerosols at a wall. *Phys. Fluids A* **4,** 825–834.

Brooke, J. W., Hanratty, T. J. & McLaughlin, J. B. 1994 Free-flight mixing and deposition of aerosols. *Phys. Fluids* **6,** 3404–3415.

Chen, M., Kontomaris, K. & McLaughlin, J. B. 1995 Dispersion, growth, and deposition of coalescing aerosols in a direct numerical simulation of turbulent channel flow. *Gas–Particle Flow* **228,** 27–32.

Clift, R., Grace, J. R. & Weber, M. E. 1978 *Bubbles, Drops and Particles.* Academic Press, New York.

Germano, M. 1992 Turbulence: the filtering approach. *J. Fluid Mech.* **238,** 325–336.

Germano, M., Piomelli, U., Moin, P. & Cabot, W. H. 1991 A dynamic subgrid-scale eddy viscosity model. *Phys. Fluids A* **3,** 1760–1765.

Ghosal, S., Lund, T. S., Moin P. & Akselovoll, K. 1994 A dynamic localization model for larg-eddy simulation of turbulent flow. *J. Fluid Mech.* **286,** 229–255.

Kallio, G. A. & Reeks, M. W. 1989 A numerical simulation of particle deposition in turbulent boundary layers. *Int. J. Multiphase Flow* **15,** 433–446.

Kim, J. & Moin, P. 1985 Application of a fractional-step method to incompressible Navier–Stokes equation. *J. Comput. Phys.* **59,** 308–323.

Kontomaris, K., Hanratty, T. J. & McLaughlin, J. B. 1992 An algorithm for tracking fluid particles in a spectral simulation of turbulent channel flow. *J. Comput. Phys.* **103,** 231–242.

Lilly, D. K. 1992 A proposed modification of the Germano subgrid-scale closure method. *Phys. Fluids A* **4,** 633–635.

Liu, B. Y. H. & Agarwal, J. K. 1974 Experimental observation of aerosol deposition in turbulent flow. *Aerosol Science* **5,** 145–155.

McCoy, D. D. & Hanratty, T. J. 1977 Rate of deposition of droplets in annular two-phase flow. *Int. J. Multiphase Flow* **3,** 319–331.

McLaughlin, J. B. 1989 Aerosol particle deposition in numerically simulated channel flow. *Phys. Fluids A* **1,** 1211–1224.

Meneveau, C., Lund, T. S. & Cabot, W. 1994 A Lagrangian dynamic subgrid-scale model of turbulence. *Proceedings of the 1994 Summer Program,* Center for Turbulence Research, Stanford University, pp. 271–300.

Perot, J. B. 1993 An analysis of the fractional step method. *J. Comput. Phys.* **108,** 51–58.

Piomelli, U. & Liu, J. 1994 Large-eddy simulation of rotating channel flows using a localized dynamic model. In *Symposium on Application of Direct and Large Eddy Simulation to Transition and Turbulence,* Chania, Greece, 18–21 April 1994.

Rouson, D. W. I. & Eaton, J. K. 1994 Direct numerical simulation of turbulent channel flow with immersed particles. *Numerical Methods in Multiphase Flows* **185,** 47–57.

Saffman, P. G. 1965 The lift on a small sphere in a slow shear flow. *J. Fluid Mech.* **22,** 385–340.

Saffman, P. G. 1968 Corrigendum to 'The lift on a small sphere in a slow shear flow'. *J. Fluid Mech.* **31,** 624.

Schumann, U. 1975 Subgrid scale model for finite difference simulations of flows in plane channels and annuli. *J. Comput. Phys.* **18,** 376–404.

Schumann, U. 1991 Subgrid length-scales for large-eddy simulation of stratified turbulence. *Theor. Comput. Fluid Dynamics* **2,** 279–290.

Squires, K. D. & Piomelli, U. 1995 Dynamic modeling of rotating turbulence. In *Turbulent Shear Flows 9* (Edited by F. Durst, N. Kasagi, B. E. Launder, F. W. Schmidt &. J. H. Whitelaw). Springer, Berlin, pp. 71–83.

Swailes, D. C. & Reeks, M. W. 1994 Particle deposition from a turbulent flow. I. A steady-state model for high inertia particles. *Phys. Fluids* **6,** 3392–3403.

Williams, G. P. 1969 Numerical integration of the three-dimensional Navier–Stokes equations for incompressible flow. *J. Fluid Mech.* **37,** 727–750.

Wu, X., Squires, K. D. & Wang, Q. 1995 On extension of the fractional step method to general curvilinear coordinate systems. *Numerical Heat Transfer* **27,** 175–194.

Yeung, P. K. & Pope, S. B. 1988 An algorithm for tracking fluid particles in numerical simulation of homogeneous turbulence. *J. Comput. Phys.* **79**, 373–416.

APPENDIX

Interpolation of Fluid Velocities

Since it is only by chance that particles are located at grid points where the Eulerian velocity field is available, interpolation from the grid to the particle position is required to obtain the fluid velocity at particle locations. Interpolation schemes were investigated using LES velocity fields of fully-developed channel flow in which 250,000 particles were randomly distributed throughout the channel. Fluid velocities were interpolated to particle positions and statistics of the fluid velocity were calculated by averaging over particles contained within slabs parallel to the wall (i.e. averaging over homogeneous x–z planes). For an accurate interpolation scheme fluid velocity statistics calculated in this manner should converge to those calculated using the fluid velocities directly available on the grid. The schemes examined in this work were linear interpolation, fourth-order, and sixth-order Lagrange polynomials. Results are shown in figures A1 and A2 for the mean and rms velocities, respectively. It is clear that all the interpolation schemes yield accurate predictions of the mean flow. However, there is a noticeable effect on the velocity fluctuations, especially in the wall-normal and spanwise directions. Consistent with results obtained by other investigators in both homogeneous turbulence and turbulent channel flow (e.g. see Yeung & Pope 1988; Balachandar & Maxey 1989; Kontomaris *et al.* 1992), the largest differences in interpolated velocities is obtained using linear interpolation. Errors in the wall-normal rms velocity are approximately 8% using linear interpolation scheme whereas the errors using the fourth-order and sixth-order Lagrange polynomials are less than 1%. Though not shown here, similar conclusions regarding the effect of interpolation on Lagrangian statistics of fluid elements are also obtained, i.e. the largest errors are obtained using linear interpolation while fourth-order Lagrange polynomials yields acceptable accuracy. Thus, based upon these findings, in this study fourth-order Lagrange polynomials were used for velocity interpolation.

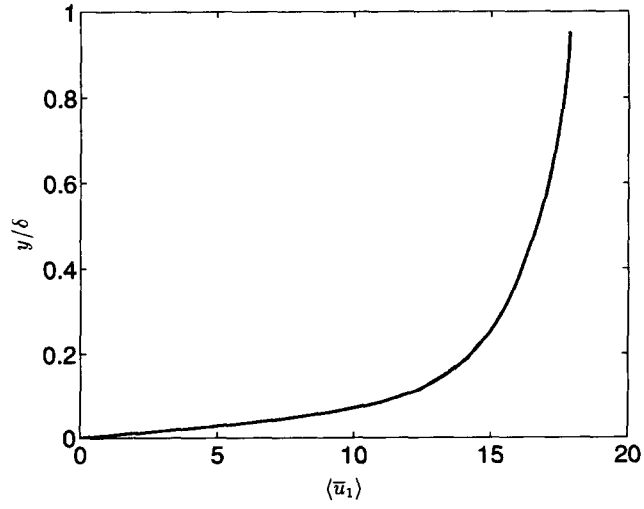

Figure A1. Effect of interpolation on mean streamwise velocity in turbulent channel flow, $Re_\tau = 180$. —— Eulerian; – – – linear interpolation; · · · 4th order Lagrange polynomials; —· — 6th-order Lagrange polynomials.

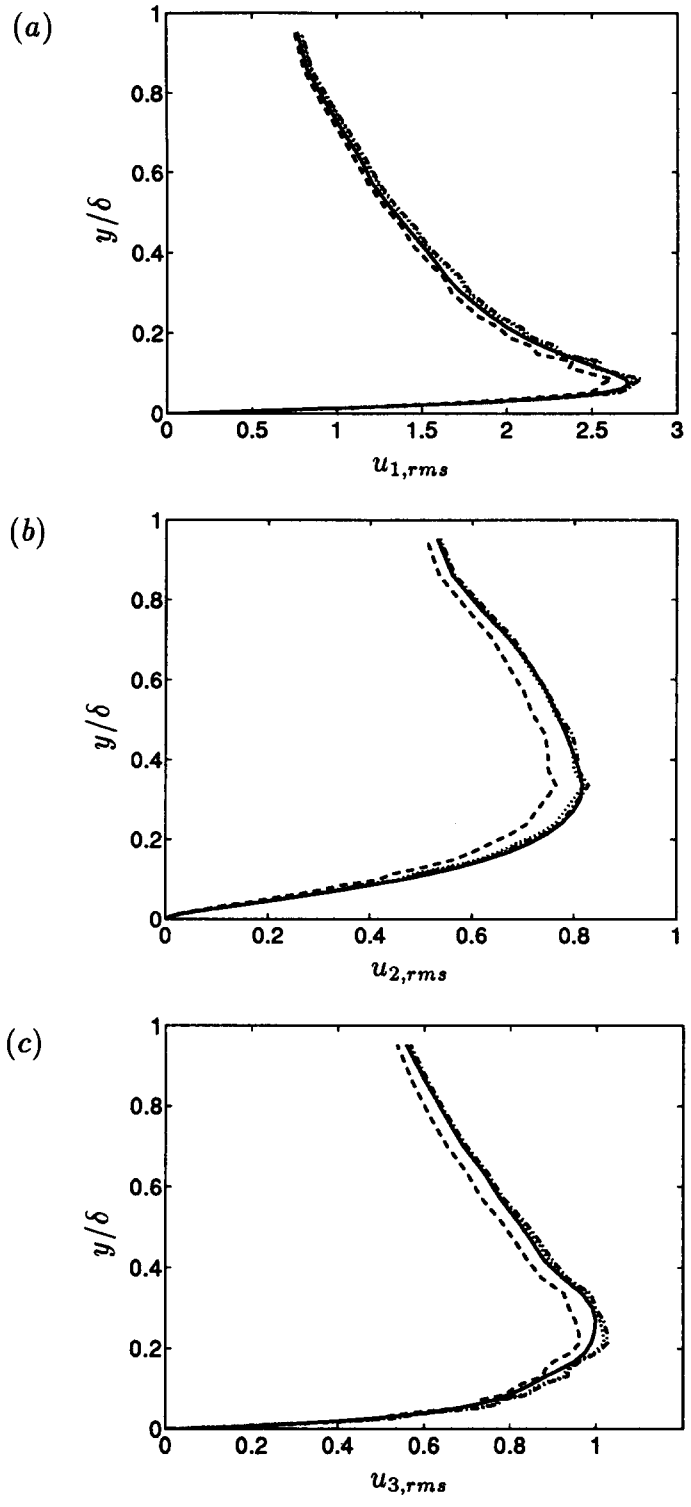

Figure A2. Effect of interpolation on the rms fluctuating velocity in turbulent channel flow, $Re_\tau = 180$. (a) streamwise; (b) wall-normal; (c) spanwise. —— Eulerian; – – – linear interpolation; · · · 4th order Lagrange polynomials; — · — 6th-order Lagrange polynomials.